Zeitschrift: Helvetica Physica Acta
Band: 58 (1985)
Heft: 2-3

Artikel: Renormalisation effects due to excitons and biexcitons in highly excited CuCl
Autor: Lévy, R. / Hönerlage, B. / Grun, J.B.
DOI: https://doi.org/10.5169/seals-115595

Helvetica Physica Acta, Vol. **58** (1985) 252–261 0018–0238/85/020252–10$1.50 + 0.20/0

Renormalisation effects due to excitons and biexcitons in highly excited CuCl

By R. Lévy, B. Hönerlage and J. B. Grun, Laboratoire de Spectroscopie et d'Optique du Corps Solide, (Associé au C.N.R.S. n° 232), 5, rue de l'Université, 6700 Strasbourg France

(19. VII. 1984)

In honor of Emanuel Mooser's 60th birthday

Abstract. We discuss dispersion and absorption anomalies which are induced by a strong light field in a three-level system like CuCl. Such anomalies are studied by different experimental techniques and may give rise to optical bistability and phase conjugation.

I. Introduction

The study of the optical nonlinear response of semiconductors under high excitation conditions by a light beam has been of increasing interest these recent years since nonlinear optical phenomena yield a wide field of applications. We are especially interested in systems like CuCl, where excitons and biexcitons exist simultaneously and can be resonantly excited by one- and two-photon absorption processes. Such systems may be reasonably well described by a three-level model [1]. If this system is excited by a strong light beam at frequency ω_p, the dielectric function is considerably modified at frequencies $\omega_t \neq \omega_p$ provided that [2, 3]

$$\hbar\omega_t + \hbar\omega_p = E_{Bi} \tag{1}$$

where E_{Bi} is the energy of the biexciton ground state. In the absence of damping, this anomaly results in an induced polariton branch which could be determined experimentally [4, 5]. This anomaly is resonant on the biexciton energy. However, non-resonant anomalies have also been observed and not yet explained [6–8]. In addition, if the frequency of the test- and pump-beam becomes degenerated, the pump beam itself is subject to the dispersion anomaly and changes its own propagation. Therefore, it was interesting to calculate the intensity dependent dielectric function including population effects and to discuss experimental results under this aspect.

II. Density matrix formulation of the dielectric function

In order to discuss results from momentum space spectroscopy, we need a description of the dielectric function in the presence of a light field A oscillating

with two frequency components ω_t and ω_p. In the dipole-approximation, the Hamiltonian of the system is given by [9, 10].

$$H = H_0 + H_{\text{int}} = H_0 - \mu A(\omega_t, \omega_p) \tag{2}$$

where H_0 is the Hamiltonian of the non-interacting system and μ the dipole-operator. The light field

$$A(\omega_t, \omega_p) = A_0^t \cos \omega_t t + A_0^p \cos \omega_p t \tag{3}$$

will be linearly polarized. Without lack of generality, the phases of both field components can be chosen equal to zero in this model. H_0 is diagonalized, having three eigenstates which are the crystal ground state with energy zero, the exciton and the biexciton states. Concerning CuCl, the interaction term induces transitions from the ground state to the exciton state and from the exciton to the biexciton state. The dipole-matrix elements are denoted by μ_{ex} and μ_{Bi}, respectively. All other transitions are forbidden. The matrix representation of the Hamiltonian then reads:

$$H_0 = \begin{pmatrix} 0 & 0 & 0 \\ 0 & E_{\text{ex}} & 0 \\ 0 & 0 & E_{\text{Bi}} \end{pmatrix}; \qquad H_{\text{int}} = -\begin{pmatrix} 0 & \mu_{\text{ex}} A & 0 \\ \mu_{\text{ex}} A & 0 & \mu_{\text{Bi}} A \\ 0 & \mu_{\text{Bi}} A & 0 \end{pmatrix} \tag{4}$$

For the sake of simplicity, μ_{ex} and μ_{Bi} are chosen to have real values. Applying the density-matrix formalism [11] in the Schrödinger picture, we can now calculate the time evolution of the transition amplitudes ρ_{ij} between the states i and j from the expression

$$\frac{\partial \rho_{ij}}{\partial t} = \frac{i}{\hbar} [\rho, H]_{ij} - \Gamma_{ij} \rho_{ij} \tag{5}$$

For $i \neq j$, Γ_{ij} is the inverse of the transverse relaxation time τ_2 which accounts for incoherent scattering. In the case of diagonal elements ($i = j$), Γ_{ii} is the inverse of the energy relaxation time τ_1 of the different quasi particles.

We are now interested in periodic solutions of the set of Bloch equations defined by equation (5) in the presence of the electric field $A(\omega_t, \omega_p)$. We therefore expand the different matrix elements ρ_{ij} into a Fourier series in ω_t and ω_p, i.e.:

$$\rho_{ij} = \sum_{nn'} \rho_{ij}^{nn'} e^{i(n\omega_t t + n'\omega_p t)} \tag{6}$$

This ansatz neglects the transient properties of the dielectric function ε, which defines, in the one-oscillator model, the resonant nonlinear susceptibility χ_{res} as:

$$\varepsilon(\mathbf{Q}_t, \omega_t)/\varepsilon_0 = \varepsilon_b + \chi_{\text{res}}(\mathbf{Q}_t, \omega_t) = \frac{\hbar^2 c^2 Q_t^2}{E_t^2(\mathbf{Q}_t)} \tag{7}$$

where ε_b is the background dielectric constant, accounting for all other oscillators. χ_{res} may now be expressed by the Fourier coefficients of the transition amplitudes and we obtain [9, 10]:

$$\chi_{\text{res}} = \frac{2N}{\varepsilon_0 A_0^t} \{\mu_{\text{ex}}(\rho_{12}^{10} + (\rho_{12}^{-10})^*) + \mu_{\text{Bi}}(\rho_{23}^{10} + (\rho_{23}^{-10})^*)\} \tag{8}$$

where N is the density of crystal atoms. The different Fourier coefficients in equation (8) are calculated from equations (5) and (6), which lead to an infinite system of linear equations in $\rho_{ij}^{nn'}$. This system may be approximated by taking into account only terms with $|n|+|n'|\leqslant 2$, which includes all resonant processes. Doing this, we avoid the rotating wave approximation [12–17] which gives generally good qualitative results at the resonance, but is not sufficient to explain results from Hyper-Raman scattering, which are obtained outside the excitonic resonance. It is worthwhile pointing out that our approximation on the order of photon processes n and n' involved is not an approximation on the field strength but on the frequency components involved.

The system of linear equations for the $\rho_{ij}^{nn'}$ is then solved numerically and the dielectric function $\varepsilon(\mathbf{Q}, \omega)$ is calculated from equations (7) and (8). Real and imaginary parts of ε are related to the polariton wavevector $\mathbf{Q}_t$ and the absorption constant α_t by the relations:

$$Q_t = \frac{\omega_t}{\sqrt{2}c}\sqrt{\mathrm{Re}\,\varepsilon + \sqrt{(\mathrm{Re}\,\varepsilon)^2 + (\mathrm{Im}\,\varepsilon)^2}} \tag{9}$$

and

$$\alpha_t = \frac{\omega_t}{\sqrt{2}c}\sqrt{-\mathrm{Re}\,\varepsilon + \sqrt{(\mathrm{Re}\,\varepsilon)^2 + (\mathrm{Im}\,\varepsilon)^2}} \tag{10}$$

where c is the vacuum light velocity. By this means, the knowledge of $\varepsilon(\mathbf{Q}_t, \omega_t)$ in the presence of an exciting pump beam at frequency ω_p allows us to determine the polariton dispersion $E_t(\mathbf{Q}_t)$. It depends on ω_p and on the density of exciting polaritons n_p.

Figure 1 gives the dispersion of the lower polariton branch for CuCl. The full line corresponds to Hopfield's one-oscillator model for vanishing damping, i.e. in the absence of any renormalization process. At low excitation intensities all dispersion curves converge towards this curve. The parameters used are well-known from two-photon absorption [18] and Hyper-Raman scattering [19]. The dashed-dotted line gives the dispersion of the test beam for low intensities (photon density $n_t \leqslant 10^{10}\,\mathrm{cm}^{-3}$) in the presence of an exciting beam at the energy $\hbar\omega_p = 3.184\,\mathrm{eV}$ and a photon density $n_p = 10^{15}\,\mathrm{cm}^{-3}$. Concerning the damping constants [9, 10], we have chosen for sake of simplicity:

$$\hbar\Gamma_{12} = \hbar\Gamma_{23} = \tfrac{1}{2}\hbar\Gamma_{13} = 2\times 10^{-4}\,\mathrm{eV} \tag{11}$$

and

$$\hbar\Gamma_{22} = \hbar\Gamma_{33} = 1.5\times 10^{-6}\,\mathrm{eV} \tag{12}$$

These values correspond to the order of magnitude for the dephasing and radiative lifetime of excitons and biexcitons estimated from two-photon absorption [18], induced absorption [20] and Hyper-Raman scattering [21] as we shall see in the next paragraph.

Two anomalies are situated at the energies $E_{\mathrm{Bi}} - \hbar\omega_p = 3.188\,\mathrm{eV}$ and $E_{\mathrm{Bi}} - E_{\mathrm{ex}} = 3.1695\,\mathrm{eV}$, where the first resonance corresponds to a two-photon absorption process of the two beams towards the biexciton state, and the second to the induced absorption from the exciton to the biexciton state. The inset shows that for the same set of parameters but, for $n_p = 10^{16}\,\mathrm{cm}^{-3}$, an anomaly is also

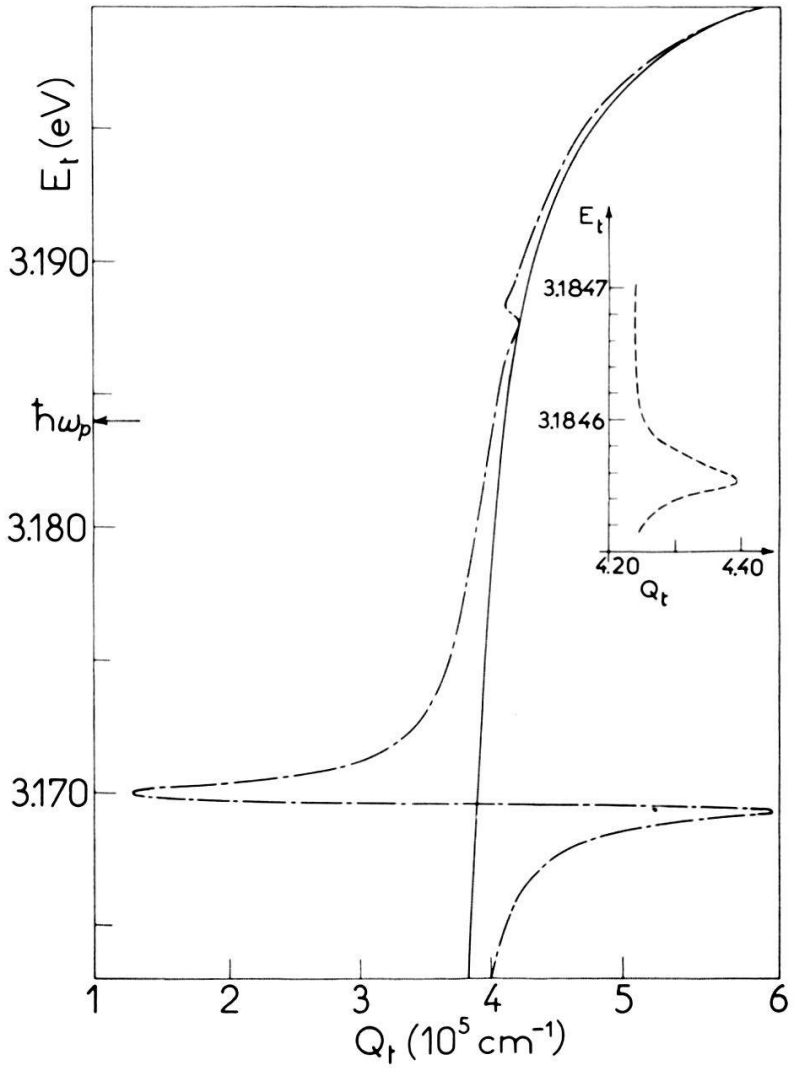

Figure 1
Polariton dispersion $E_t(\mathbf{Q}_t)$ of CuCl when excited at $\hbar\omega_p = 3.184\,\text{eV}$ by a pump beam with $n_p = 10^{15}\,\text{cm}^{-3}$. The full line gives the result without renormalization. The inset shows the pseudo-resonance near $\hbar\omega_p$ for $n_p = 10^{16}\,\text{cm}^{-3}$.

observed near the frequency of the pump beam. This quasi-resonance is Stark-shifted and is due to the slowly varying frequency components in the exciton and biexciton populations. It is only present at very high excitation densities. It is interesting to notice that the latter resonances vanish if the population of excitons and biexcitons is equal to zero.

Figure 2 shows the absorption coefficient α_t for the same set of parameters. Again, the absorption shows maxima at the two energetic values mentioned above. An absorption increase around the energy of the pump beam is not important. The increase of α_t around 3.2 eV is due to the exciton absorption, which is not covered here.

The dispersion and absorption anomalies discussed above increase with increasing excitation intensity n_p and decreasing damping constants Γ_{12}.

It is evident that if the frequencies of the test and pump beams becomes degenerated, we have the situation where the dispersion and absorption of a single beam is modified by its own intensity. This effect has been discussed theoretically in Ref. 2, 3, 12–17 by different approaches. Since we have seen

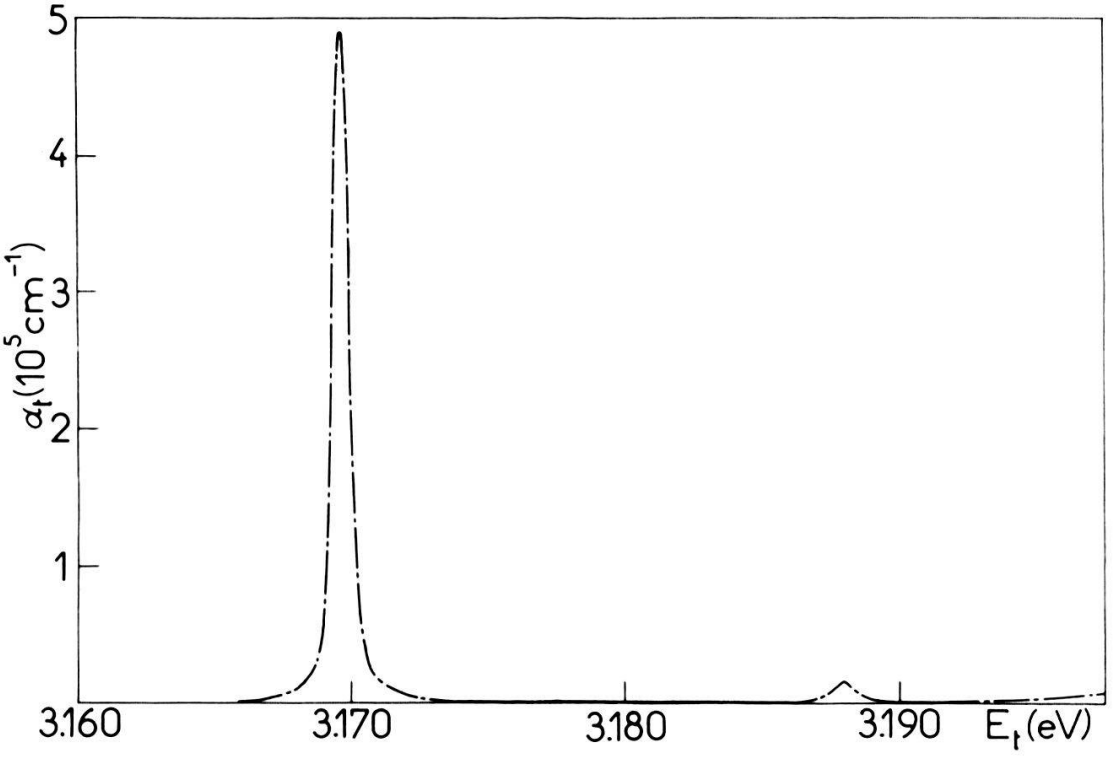

Figure 2
Absorption coefficient $\alpha_t(E_t)$ for the same situation as in Fig. 1.

above that finite population effects may modify the dispersion and absorption properties, we have examined this situation [22], using the density matrix formalism and the Fourier analysis of the different ρ_{ij}. Since the system is much simpler than the case of the two fields, it may be handled by continuous matrix inversion [23]. This method allows us to include all types of non-resonant transitions, which have been neglected before [9, 10]. Thus we could check our approximations and give a dielectric function which includes proper contributions of a non-resonant background.

III. Experimental results and discussions

Let us briefly describe how the Hyper-Raman scattering process can be used to study the anomalies of the lower polariton branch, shown in Fig. 1. This polariton branch is represented in Fig. 3 in two dimensions in the absence of renormalization effects. In the Hyper-Raman diffusion process [24], two laser photons propagating inside the crystal as polaritons with wave vector $\mathbf{q}_l$, virtually excite a biexciton. The biexciton serving as an almost resonant intermediate state decays into two polaritons $E_i(\mathbf{q})$ and $E_j(\mathbf{k})$. No relaxations are taking place on the intermeditate states. Therefore, momentum and energy are conserved in the process, as shown in Fig. 3:

$$\begin{aligned} 2\mathbf{q}_l &= \mathbf{q}+\mathbf{k} \\ 2\hbar\omega_l &= E_i(\mathbf{q})+E_j(\mathbf{k}) \end{aligned} \tag{13}$$

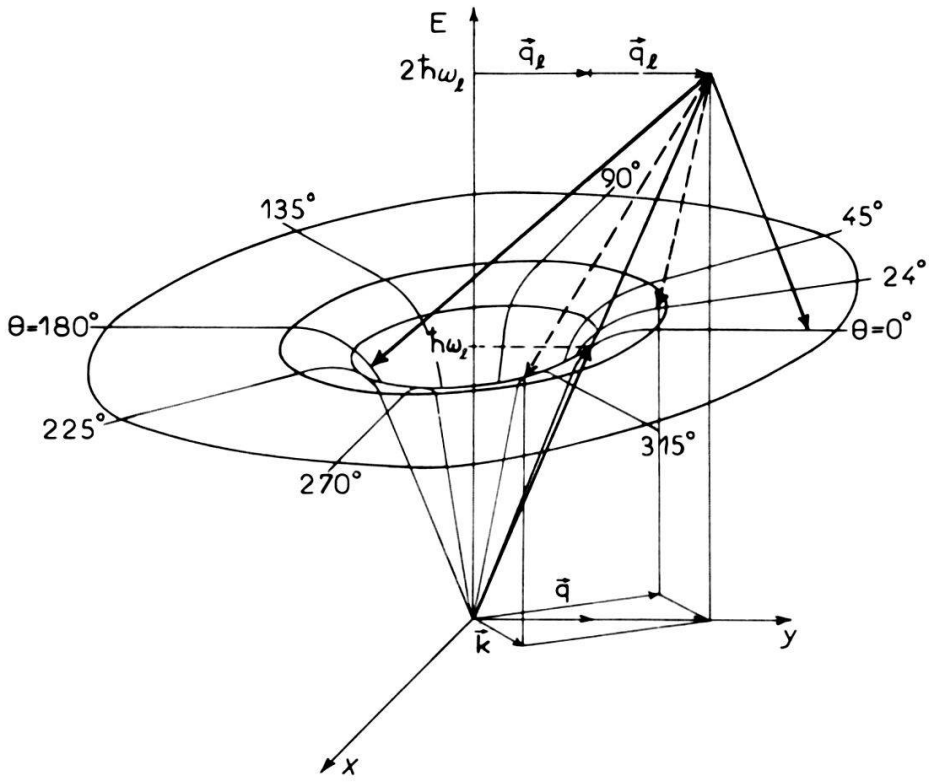

Figure 3
Resonant Hyper-Raman scattering involving the lower polariton branch in the absence of renormalization effects.

In the experiments described here, the two emitted polaritons belong to the lower branch of the dispersion curve. One ($E_i(\mathbf{q})$) is observed, the other one ($E_j(\mathbf{k})$) is not detected. $E_i(\mathbf{q})$ changes its energy when $\hbar\omega_l$ is tuned.

As shown in Fig. 3, θ is the scattering angle between incident and observed polaritons. Small θ ($\theta < 30°$) correspond to a forward scattering configuration where the excited surface is observed through the sample. Since the emitted polaritons, represented by the dotted arrows of Fig. 3, lie in the region of the dispersion curve we are interested in, we shall use this experimental configuration in these experiments. In this case, three recombination channels exist for one given direction of excitation. Only two channels (R_T^+ and R_T^-) will be studied here. For completeness, let us add that for large scattering angles θ corresponding to a backward scattering configuration, the excited surface is directly observed. In that case, one of the polaritons is exciton-like, the other, polariton-like. The final states are indicated by the full arrows in Fig. 3.

In these experiments, the photon energy $\hbar\omega_l$ of the exciting laser and the energies E_i of the emitted Hyper-Raman lines (R_T^+ and R_T^-) are measured as well as the angle of incidence α of the exciting beam and the angle of observation β. If we can calculate, either analytically or numerically, the theoretical dispersion, we can fit the experimental values of E_i with calculated ones, by adjusting, in a self-consistent way, the different unknown parameters of the dispersion.

The experimental set-up used is shown in Fig. 4. The samples are excited by the tunable light of a grazing incidence dye laser (αNND in ethanol or BBQ in toluen), pumped by a Lambda-Physik excimer laser. The laser intensity is kept below 5 MW/cm^2. The spectral width of the laser light is 0.03 meV. The samples

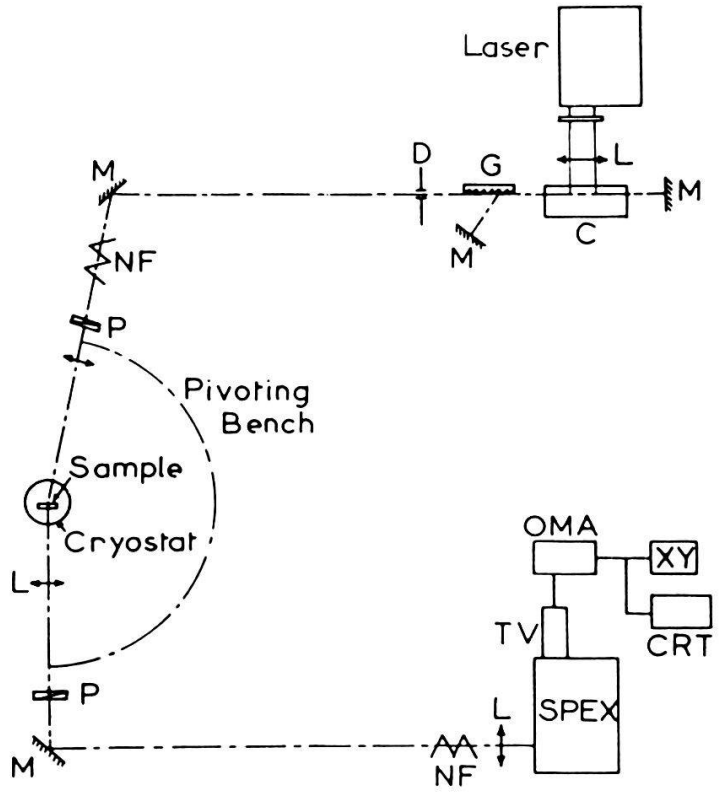

Figure 4
Set-up for Hyper-Raman scattering experiments. Laser: Excimer laser; M: Mirror; C: dye Cell; D: Diaphragm; NF: Neutral Density Filter; HP: Polarizer; G: Grating; OMA: Optical Multichannel Analyser; TV: SIT Picture Tube; Spex: Spectrograph.

studied are high purity platelets of CuCl crystals cooled down to pumped liquid helium temperature. The forward scattering configuration of the experiment is shown in Fig. 4. The emitted light is recorded, through a 3/4m spex spectrograph, by a PAR optical multichannel analyzer system.

Figures 5 and 6 represent the spectral positions of the Hyper-Raman emission lines R_T^+ and R_T^- as functions of the energy $\hbar\omega_l$ of the exciting photons in two different forward scattering configurations [4]. The angle of incidence α is equal to zero in both cases, the angles of observation β are 11° and 23°, respectively.

We have made a numerical adjustment between HR line positions R_T^+ and R_T^- and calculated ones. A very good fit has been obtained as shown in Fig. 5, where the calculated positions are represented by a continuous curve using the following parameters: a density of photons $n_p = 4.3 \times 10^{14}\,\mathrm{cm}^{-3}$, a dephasing constant $\hbar\Gamma_{12} = 3 \times 10^{-4}$ eV and an arbitrarily chosen value of $\hbar/\tau = 1.5 \times 10^{-6}$ eV.

The global shift between experimental HR line positions and the dotted line representing the positions obtained previously, is now well reproduced. This shift is due to the intensity dependence of the background dielectric constant.

The induced polariton branch due to the two-photon biexciton absorption of a photon $\hbar\omega_l$ of the exciting laser and a photon emitted ($\hbar\omega_i$ or $\hbar\omega_j$), is also well taken into account as shown by the good fit between experimental results and the calculated continuous curve. This induced branch which corresponds to a splitting of the Hyper-Raman lines is observed around the frequencies:

$$\hbar\omega_i = E_{Bi} - \hbar\omega_l \quad \text{and} \quad \hbar\omega_i = 3\hbar h\omega_l - E_{Bi}$$

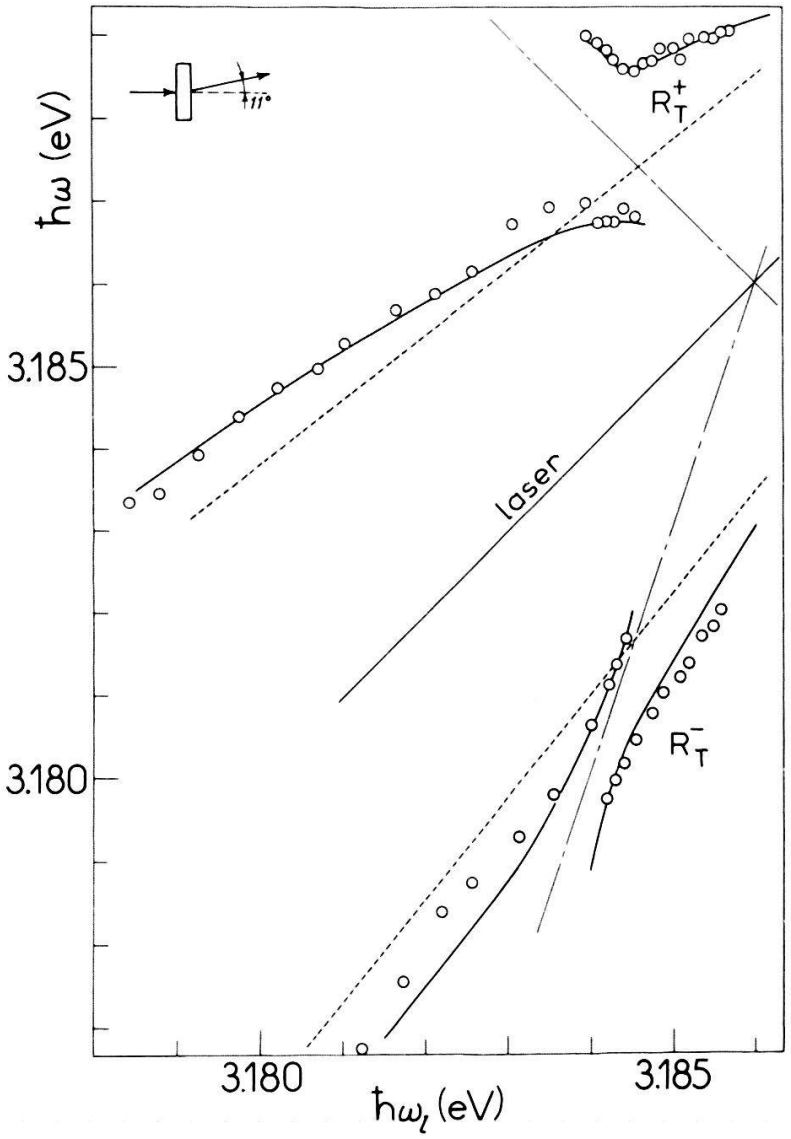

Figure 5
Experimental positions of Hyper-Raman emission lines of CuCl when excited under an angle of incidence $\alpha = 0°$ and for a direction of observation $\beta = 11°$.

using the equations (13), represented by the dashed-dotted lines drawn in Fig. 5.

In Fig. 6, the calculated spectral positions of the HR emission lines represented by the continuous curve correspond to an excitation intensity of $n_p = 10^{15}\,\mathrm{cm}^{-3}$ and fixed inverse energy relaxation times Γ_{22} and Γ_{33} equal to $2\times 10^{-5}\,\mathrm{eV}$. Again, the overall shift of the HR lines is satisfactorily explained. Besides the shift and the splitting of the HR lines, we also observe a non-linear shift when the photon energy of the exciting laser is tuned across half the biexciton energy [25, 26].

The same information may be obtained by non-degenerate, non-collinear four-wave mixing [5, 27]. Similar to electronic CARS, it is the stimulated process [28] corresponding to hyper-Raman scattering as the spontaneous one. In addition, a different technique using the laser induced birefringence of the crystal [29, 30] has also been developed.

If a single laser beam excites the crystal, the polariton dispersion is also

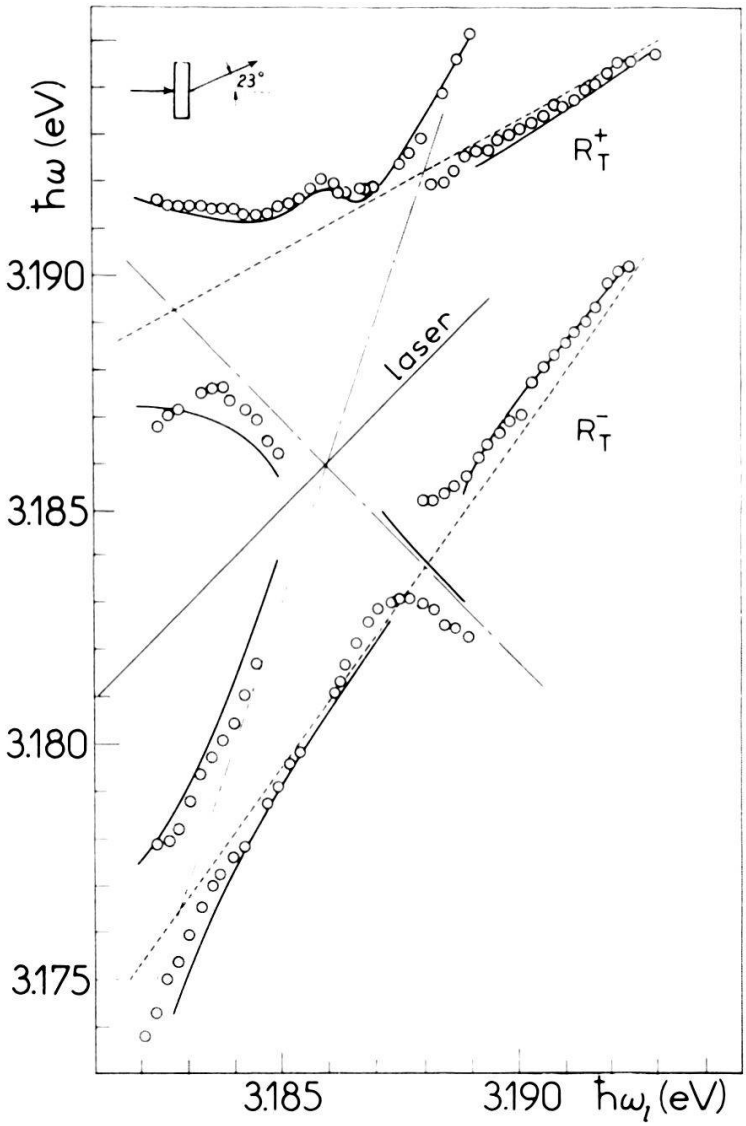

Figure 6
Experimental positions of Hyper-Raman emission lines of CuCl when excited under an angle of incidence $\alpha = 0°$ and for a direction of observation $\beta = 23°$.

modified, leading to a strong anomaly near half the biexciton energy [12–15, 22]. As it has been pointed out in Ref. 31, 32, this anomaly can be used to obtain optical bistability, if sufficient feedback is provided. This has recently been demonstrated [33, 34], using CuCl crystals inside a Fabry–Perot cavity. The switching times of this device have been demonstrated to be below 500 ps, if biexcitons are created only virtually.

Conclusion

Concentrating on CuCl, we have discussed here different anomalies of the polariton dispersion. The origin of these anomalies is due to the simultaneous existence of excitons and biexcitons. They lead to important applications such as optical bistability and phase conjugation.

Acknowledgements

The authors are grateful to J. Y. Bigot and F. Tomasini for assistance in doing experiments and numerical calculations. This work has been supported by a contract with the 'Ministère des PTT' of France, 'Direction Générale des Télécommunications', 'Direction des Affaires Industrielles et Internationales'.

It has also been carried out in the framework of an operation launched by the Commission of the European Communities under the experimental phase of the European Community Stimulation Action (1983–1985).

REFERENCES

[1] For a recent review, see: J. B. GRUN, B. HÖNERLAGE and R. LÉVY in 'Excitons', E. I. Rashba and M. D. Sturge editors, North Holland Pub. Corp., Amsterdam (1982), and references cited therein.
[2] R. MÄRZ, S. SCHMITT-RINK and H. HAUG, Z. Physik *B40*, 9 (1980).
[3] V. MAY, K. HENNEBERGER and F. HENNEBERGER, Phys. Stat. Sol. (b), *94*, 611 (1979).
[4] J. B. GRUN, B. HÖNERLAGE and R. LÉVY, Solid State Comm., *46*, 51 (1983).
[5] B. HÖNERLAGE, J. Y. BIGOT, R. LÉVY, F. TOMASINI and J. B. GRUN, Solid State Comm. *48*, 803 (1983).
[6] K. KEMPF, G. SCHMIEDER, G. KURTZE and C. KLINGSHIRN, Phys. Stat. Sol. (b), *107*, 297 (1981).
[7] I. BROSER, private communication.
[8] A. BIVAS, VU DUY PHACH, B. HÖNERLAGE and J. B. GRUN, Phys. Stat. Sol. (b), *84*, 235 (1977).
[9] J. Y. BIGOT and B. HÖNERLAGE, Phys. Stat. Sol. (b) *121*, 649 (1984).
[10] B. HÖNERLAGE and J. Y. BIGOT, Phys. Stat. Sol. (b) *123*, 201 (1984).
[11] A. YARIF, 'Quantum Electronics', 2nd edition, Wiley and Sons, New York (1975).
[12] I. ABRAM and A. MARUANI, Phys. Rev. *B26*, 4759 (1982).
[13] C. C. SUNG and C. M. BOWDEN in 'Tropical Meeting on Optical Bistability', Rochester (USA), 1983.
[14] F. HENNEBERGER and V. MAY, Phys. Stat. Sol. (b) *109*, K 139 (1982).
[15] E. HANAMURA, Solid State Comm., *38*, 939 (1981).
[16] T. TOKIHIRO and E. HANAMURA, Progr. Theor., Phys. Supp. *69*, 451 (1980).
[17] G. P. AGRAWAL and H. J. CARMICHAEL, Phys. Rev., *A19*, 2074 (1979).
[18] VU DUY PHACH, A. BIVAS, B. HÖNERLAGE and J. B. GRUN, Phys. Stat. Sol. (b) *84*, 731 (1977).
[19] B. HÖNERLAGE, A. BIVAS and VU DUY PHACH, Phys. Rev. Letters *41*, 49 (1978).
[20] R. LÉVY, B. HÖNERLAGE and J. B. GRUN, Phys. Rev. *B19*, 2326 (1979).
[21] VU DUY PHACH, A. BIVAS, B. HÖNERLAGE and J. B. GRUN, Phys. Stat. Sol. (b) *86*, 159 (1978).
[22] B. HÖNERLAGE and J. Y. BIGOT, Phys. Stat. Sol. (b) *124*, 221 (1984).
[23] H. RISKEN and H. D. VOLLMER, Z. Physik *B39*, 339 (1980).
[24] J. B. GRUN, Proc. 15th Int. Conference, Physics of Semiconductors, Kyoto, 1980.
[25] T. ITOH, T. SUZUKI and M. UETA, J. Phys. Soc. Japan *44*, 345 (1978).
[26] T. ITOH and T. SUZUKI, J. Phys. Soc. Japan *45*, 1939 (1978).
[27] B. HÖNERLAGE, R. LÉVY and J. B. GRUN, Opt. Comm., *43*, 443 (1982).
[28] A. MARUANI, J. L. OUDAR, E. BATIFOL and D. S. CHELMA, Phys. Rev. Letters, *41*, 20 (1978).
[29] M. KUWATA and N. NAGASAWA, J. Phys. Soc. Japan *51*, 2591 (1982).
[30] M. KUWATA, T. MITA and N. NAGASAWA, Sol. State Comm., *40*, 911 (1981).
[31] E. HANAMURA, Sol. State Comm., *38*, 939 (1981).
[32] S. W. KOCH and H. HAUG, Phys. Rev. Letters *46*, 450 (1981).
[33] R. LÉVY, J. Y. BIGOT, B. HÖNERLAGE, F. TOMASINI and J. B. GRUN, Sol. State Comm., *48*, 705 (1983).
[34] N. PEYGHAMBARIAN, H. M. GIBBS, M. C. RASHFORD and D. A. WEINBERGER, Phys. Rev. Letters, *51*, 1692 (1983).